

El Mayor Postseismic

Trevor Hines

March 14, 2016

Introduction

Previous studies which have modeled postseismic deformation following the El Mayor-Cucapah earthquake include [Pollitz et al., 2012], [Gonzalez-ortega et al., 2014], [Spinler et al., 2015], and [Rollins et al., 2015]. [Gonzalez-ortega et al., 2014] was able to describe five months of near field ($\lesssim 50$ km from the epicenter) postseismic defomation observed by InSAR and campaign GPS with afterslip and fault contraction on the coseismically ruptured fault. [Gonzalez-ortega et al., 2014] also noted that their preferred model underestimated the GPS displacements for stations $\gtrsim 25$ km from the rupture and suggested that it could be the result of unmodeled viscoelastic relaxation. Using continuous GPS stations within 200 km of the El Mayor-Cucapah epicent, which consists mostly of stations north of the US-Mexico border, [Rollins et al., 2015] found that three years of postseismic deformation can be adequately explained by afterslip in an elastic lithosphere, albeit with an implausibly large amount of afterslip inferred on the least constrained southern most fault segment which may be acting as a proxy for distributed relaxation in the lower crust or upper mantle. In this paper, we reiterate this finding by [Rollins et al., 2015] and note that a purely elastic dislocation model is incapable of describing deformation observed at GPS stations greater than 200 km from the El Mayor-Cucapah epicenter.

Given the inability to describe both near and far field deformation with fault slip in an elastic lithosphere, [Pollitz et al., 2012], [Rollins et al., 2015] and [Spinler et al., 2015] have explored viscoelastic relaxation in the lower crust and upper mantle as a potential deformation mechanism. The lithospheric rheology is largely unknown and so modeling postseismic deformation with viscoelastic relaxation requires one to assume a rheologic model and find the best fitting model parameters, which is generally a computationally expensive nonlinear inverse problem. Consequently, a simplified structure for the lithosphere must be made to minimize the number of rheologic parameters that need to be estimated. For example, it is commonly assumed that the lithosphere consists of only three homogeneously Maxwell viscoelastic layers, which may be an inadequate representation of the lithosphere [Hines and Hetland, 2013][Riva and Govers, 2009]. Additionally, it is necessary to make simplifying assumptions about the nature of afterslip. For example [Pollitz et al., 2012] and [Spinler et al., 2015] assumed that afterslip does not persist beyond six months and one year respectively and subsequent displacements were assumed to be the result of only viscoelastic

relaxation. However, numerous observations of interseismic fault creep has been recognized in this and similar tectonic settings and it has been speculated that such creep can be initiated as a postseismic process [Çakir et al., 2012] [Cetin et al., 2014]. We are unaware of any oIn this study, we therefore do not make to implicit assumption that afterslip terminates after a given amount of time. Indeed, the preferred viscoelastic model from [Pollitz et al., 2012] underpredicts near field velocities, which could be indicative of unmodeled continued afterslip.

All of the aforementioned studies model displacements observed at stations within 200 km of the El Mayor-Cucapah epicenter, while postseismic deformation in this region following previous earthquakes of similar magnitude has been observed at distances extended out to about 300 km [Freed et al., 2007]. In the present study we examine stations within 400 km of the El Mayor-Cucapah epicenter, which turns out to be crucial for discerning the postseismic deformation mechanism.

Clearly, both afterslip and viscoelastic relaxation are involved in postseismic deformation neglecting to model one of these deformation mechanisms could result in a biased estimate of the other. In this paper we use the inverse method described in [Hines and Hetland, 2015] to estimate the afterslip an effective viscosity necessary to describe the transience postseismic deformation over the first ten months after the El Mayor-Cucapah earthquake. We then form a suite of models which have various lithospheric rheologies but viscosities that are consistent with the effective viscosity estimated from the early postseismic deformation. Of the suite of models tested, we find that five years of postseismic deformation can be explained by a combination of sustained afterslip on the coseismically ruptured fault and a Zener rheology upper mantle with viscosity that decays from 4×10^{18} to 1×10^{18} Pa s.

Data Processing

We use continuous GPS position time series provided by University Navstar Consortium (UNAVCO) for Plate Boundary Observatory (PBO) stations within a 400 km radius about the El Mayor-Cucapah epicenter. Our analysis is on the coseismic and postseismic deformation resulting from the EMC earthquake, which we collectively describe as $u(t)$. We consider GPS position time series, $u_{\text{obs}}(t)$, to be the superposition of $u(t)$, secular tectonic deformation, annual and semi-annual fluctuations, and coseismic offsets from significant earthquakes over the time span of this study. The June 14, 2010 Mw5.8 Ocotillo earthquake and the August 26, 2012 Brawley swarm, which consisted of a Mw5.5 and Mw5.3 event, are the only earthquakes after the EMC earthquake that produced noticeable offsets recorded by GPS. Although the Ocotillo earthquake had its own series of aftershocks (Haukson), neither earthquake produced transient deformation that is detectable with GPS. We thus model $u_{\text{obs}}(t)$ as

$$u_{\text{obs}}(t) = u_{\text{pred}}(t) + \epsilon \quad (1)$$

where

$$\begin{aligned} u_{\text{pred}}(t) = & u(t) + c_0 + c_1 t + \\ & c_2 \sin(2\pi t) + c_3 \cos(2\pi t) + c_4 \sin(4\pi t) + c_5 \cos(4\pi t) + \\ & c_6 H(t - t_{\text{oc}}) + c_7 H(t - t_{\text{bs}}). \end{aligned} \quad (2)$$

In the above equations, t_{oc} and t_{bs} are the times of the Ocotillo earthquake and Brawley swarm respectively, $H(t)$ is the Heaviside function, c_0 through c_7 are unknown coefficients, and ϵ is noise with zero mean and variance that assumed known.

Stations which recorded signals that clearly cannot be described by the aforementioned processes are not included in our analysis. This includes stations in the Los Angeles basin, which record deformation that is largely anthropogenic. In order to ensure an accurate estimation of the secular deformation, we only use stations that were installed at least six months prior to El Mayor-Cucapah earthquake. While several stations were installed after the EMC earthquake to improve the spatial resolution of postseismic deformation [Spinler et al., 2015], our inverse method uses postseismic displacements rather than velocities (e.g. ...), which requires the knowledge of the stations preseismic position. Despite our inability to utilize potentially rich data, we prefer to use postseismic displacements rather than potentially dubious estimates of postseismic velocities.

The October 16, 1999 Hector Mine earthquake, which occurred within our study region about 270 km north of the EMC epicenter, has produced transient postseismic deformation which we do not wish to model either mechanically or through empirical line fitting. We thus restrict our analysis to deformation observed six years after the Hector Mine earthquake, past which point postseismic deformation for nearfield sites occurs at an approximately steady rate [Savage and Svart, 2009]. When considering stations further away from the Hector Mine epicenter, postseismic transience persists for only about two years [Spinler et al., 2015].

We do not assume a parametric form for $u(t)$, (e.g. [Rollins et al., 2015]), but rather we model $u(t)$ as integrated Brownian motion, so that

$$\dot{u}(t) = \sigma^2 \int_0^t w(s) ds. \quad (3)$$

where $w(t)$ is white noise and the variance of $\dot{u}(t)$ increases linearly with time by a factor of σ^2 . We use a Kalman filtering approach to estimate $u(t)$ and the unknown parameters in eq. 2 which we describe now. In the context of Kalman filtering, our time varying state vector is

$$\mathbf{X}(t) = [u(t), \dot{u}(t), c_0, \dots, c_7] \quad (4)$$

and eq. 2 is the observation function which maps the state vector to the GPS observations. We initiate the Kalman filter by assuming a prior estimate of $\mathbf{X}(t)$ at time t_0 which has a sufficiently large covariance to effectively make our prior uninformed. For each time epoch, t_i , Bayesian linear regression is used to incorporate GPS derived estimates of displacement with our prior estimate of the state, $\mathbf{X}_{i|i-1}$, to form a posterior estimate of the state, $\mathbf{X}_{i|i}$, which has covariance $\Sigma_{i|i}$.

We then use the posterior estimate of the state at time t_i to form a prior estimate of the state at time t_{i+1} through the transition function

$$\mathbf{X}_{i+1|i} = \mathbf{F}_{i+1} \mathbf{X}_{i|i} + \delta_{i+1} \quad (5)$$

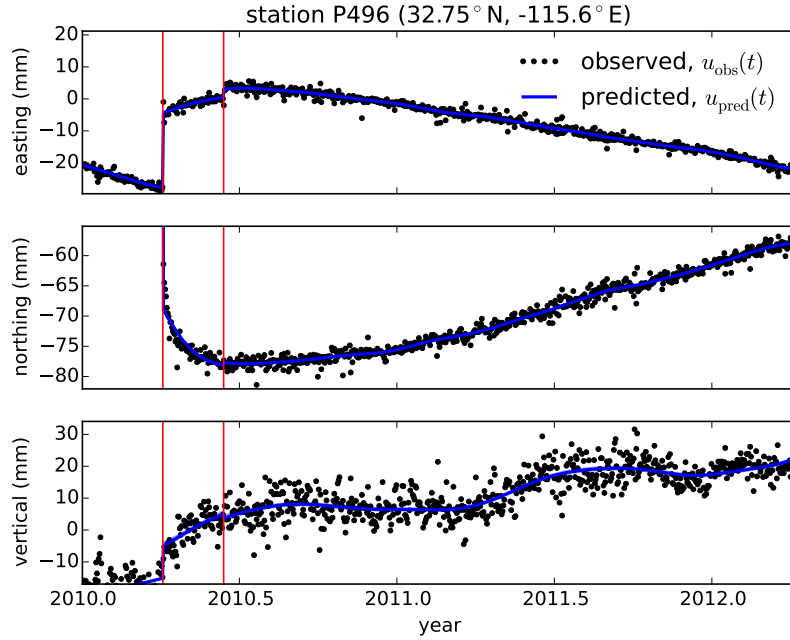


Figure 1: GPS displacement solution from UNAVCO (black) and predicted displacements after applying a Kalman filter where $\sigma^2 = 0.05 \text{m}^2/\text{yr}^3$. Red line indicates the time of the Ocotillo earthquake where a jump in the time series is estimated

where

$$\mathbf{F}_{i+1} = \begin{bmatrix} 1 & (t_{i+1} - t_i) & \mathbf{0} \\ 0 & 1 & \mathbf{0} \\ \mathbf{0} & \mathbf{0} & \mathbf{I} \end{bmatrix} \quad (6)$$

and δ_{i+1} is the process noise, which has zero mean and covariance described by

$$\mathbf{Q}_{i+1} = \sigma^2 \begin{bmatrix} \frac{(t_{i+1}-t_i)^3}{3} & \frac{(t_{i+1}-t_i)^2}{2} & \mathbf{0} \\ \frac{(t_{i+1}-t_i)^2}{2} & (t_{i+1} - t_i) & \mathbf{0} \\ \mathbf{0} & \mathbf{0} & \mathbf{0} \end{bmatrix}. \quad (7)$$

The covariance of the new prior state, $\mathbf{X}_{i+1|i}$, is then described by

$$\Sigma_{i+1|i} = \mathbf{F}_{i+1} \Sigma_{i|i} \mathbf{F}_{i+1}^T + \mathbf{Q}_{i+1}. \quad (8)$$

This process is repeated for each of the N time epochs at which point we use Rauch-Tung-Striebel smoothing to find $X_{i|N}$, which is an estimate of the state at time t_i that incorporates all N GPS observation. Our final estimates of $u(t)$ are used in subsequent analysis, while the remaining components of the state vector are considered nuisance parameters. In the interests of computational tractability, we down sample our smoothed time series from daily solutions down to weekly solutions.

The smoothness of $u(t)$ is controlled by the chosen value of σ^2 , which describes how rapidly we expect the postseismic signal to vary over time. Setting σ^2 equal to zero will

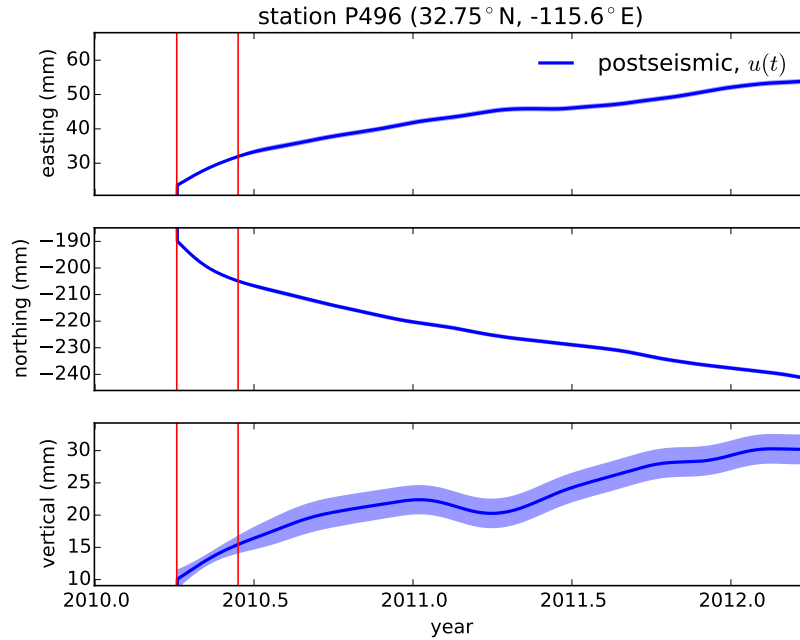


Figure 2: Postseismic displacements estimated after applying a Kalman filter to the GPS displacement solution from UNAVCO. Displacements shown have had a background secular trend removed as well as an estimated seasonal signal.

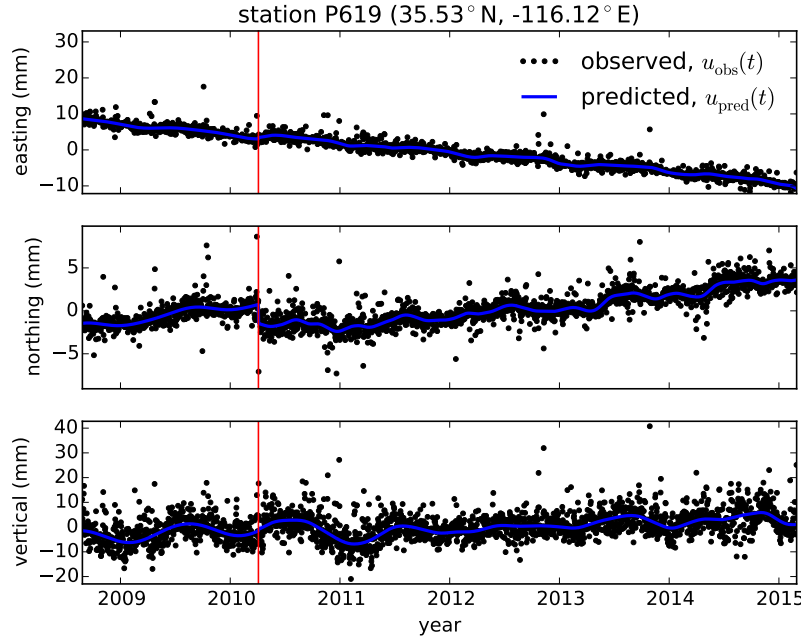


Figure 3: GPS displacement solution from UNAVCO (black) and predicted displacements after applying a Kalman filter where $\sigma^2 = 0.05\text{m}^2/\text{yr}^3$. Red line indicates the time of the Ocotillo earthquake where a jump in the time series is estimated

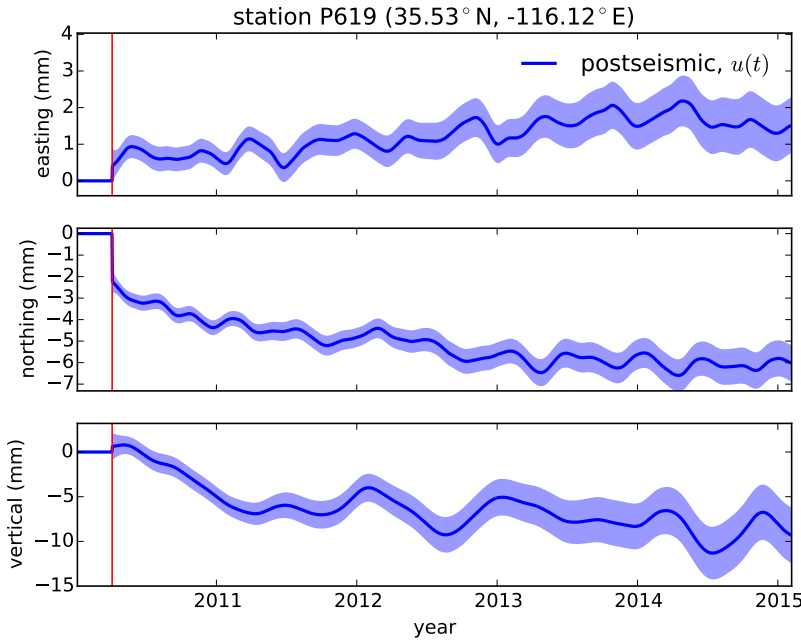


Figure 4: Postseismic displacements estimated after applying a Kalman filter to the GPS displacement solution from UNAVCO. Displacements shown do not include the estimated secular trend, seasonal signals, and displacements resulting from the Ocotillo earthquake.

effectively result in modeling $u(t)$ as a straight line which is insufficient to describe the expected transient behavior in postseismic deformation [Savage et al., 2005]. The other end-member, where σ^2 is infinitely large, will result in $u_{\text{pred}}(t)$ fitting what is obviously noise in the data. While one can use a maximum likelihood based approach to picking σ^2 (e.g. [Segall and Mathews, 1997]), we rather take a subjective approach and choose a value for σ^2 , which is used when filtering time series for each station, that is just large enough to faithfully describes the early rapid rate of postseismic deformation at the most near field station in our study, P496. This ensures that σ^2 will be sufficiently large so that our estimate of $u(t)$ does not smooth out potentially valuable postseismic signal. We find that when using $\sigma^2 = 0.05 \text{ m}^2/\text{yr}^3$, we are able to adequately describe all but the first week of postseismic deformation at station P496, which gets incorporated into our estimate of coseismic displacements (figure 1). Since we assume that the first week of deformation is overwhelmingly the result of afterslip, any unmodeled afterslip over the first week following the El Mayor-Cucapah earthquake will be added into our estimates of coseismic slip in section (). Figure 2 shows the estimate of coseismic and postseismic deformation, $u(t)$, for station P496 along with its formal uncertainties.

It is important to note that the shown uncertainties in $u(t)$ do not account for our uncertainty in eq. 2. For example, we assume that the background rate of deformation can be approximated as having a constant rate, while mechanical models would suggest this to not be true on earthquake cycle timescales [Thatcher, 1983]. Although based on inspection, assuming a constant rate of background deformation appears to be appropriate

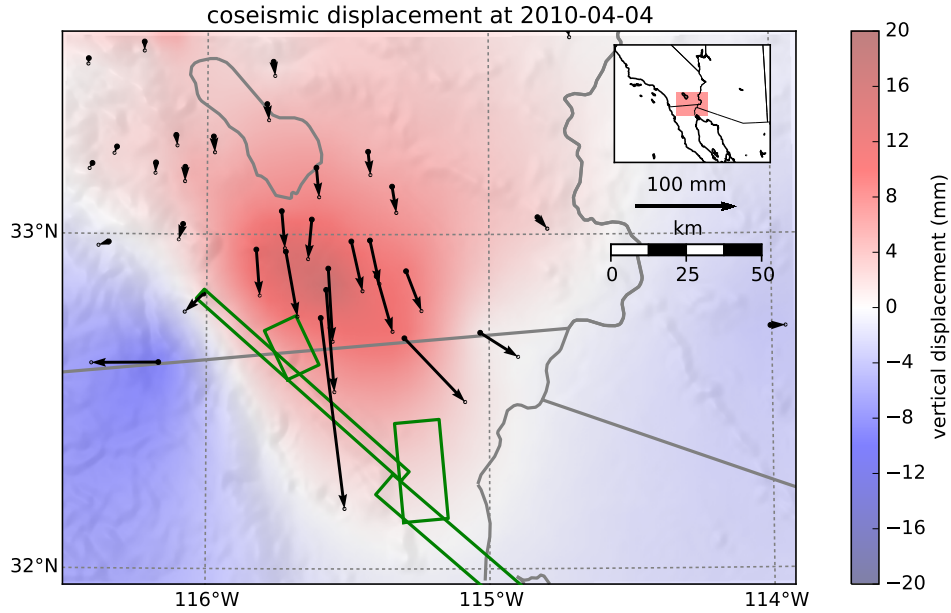


Figure 5: near field coseismic

for all stations except for perhaps the stations closest to the Hector Mine epicenter, where postseismic deformation persists. Also, our model for seasonal deformation in eq. 2 assumes a constant amplitude over time, which means that years of particularly heavy or light rainfall cannot be adequately described. This deficiency in our seasonal model causes our estimate of $u(t)$ to describe some of the unmodeled oscillations (figure 4).

note that stations jumps are only estimated for stations within 40 km of BS or OC
Cite Freed 2007 for far reaching postseismic after Landers/Hector Mine.

We show the difference in $u(t)$ for each station from 0 to 0.8 years (figure 6 and 10), 0.8 to 3.2 years (figure 7 and 11), and from 3.2 to 5.0 years (figure 8 and 12). For far field stations (figure 10, 11, and 12), we can see a clear south trending displacement throughout the first 3.2 years in stations as far as 400 km from of the El Mayor Cucapah epicenter. These displacements are most pronounced along the direction of the El Mayor-Cucapah P and S axis, as would be expected for postseismic deformation. Beyond 3.2 years, The southward trending far field postseismic deformation is barely perceptible. There is however, an eastward trend in far field stations just west of the Hector Mine epicenter. We suspect this this deformation, which is inconsistent with the pattern expected for El Mayor-Postseismic, is the result of continued transient postseismic deformation following the Hector Mine earthquake. The vertical deformation in the far field is difficult to attribute to postseismic processes. Most far field stations display an initial subsidence for the first year after the El Mayor-Cucapah earthquake followed by continued uplift. This trend in vertical deformation can be observed in all three of the quadrants where postseismic data is available, which means that the vertical deformation does not exhibit an anti-symmetric quadrant pattern, as would be expected for postseismic processes. Although we use vertical deformation in our subsequent

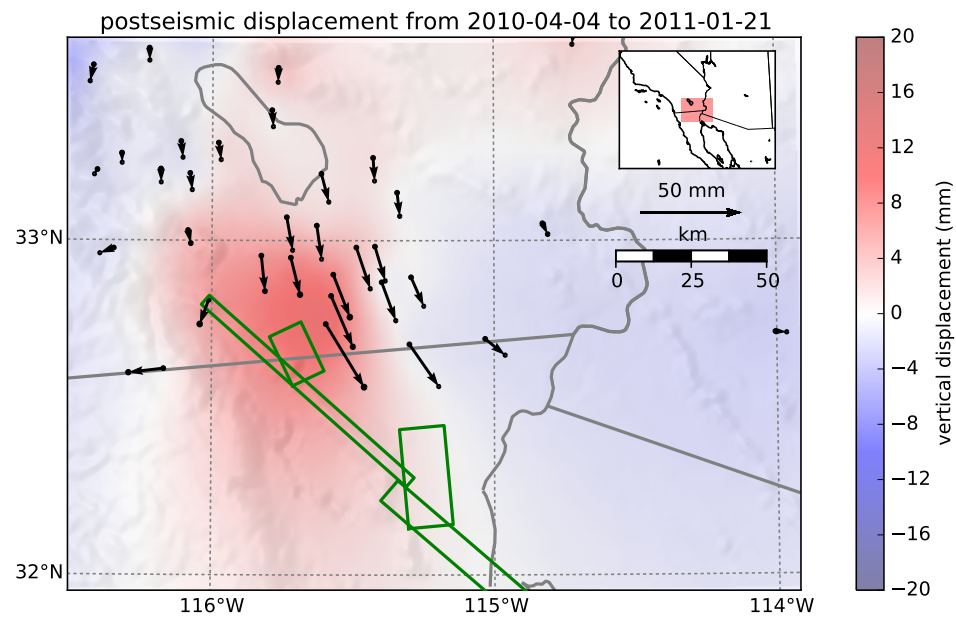


Figure 6: near field coseismic

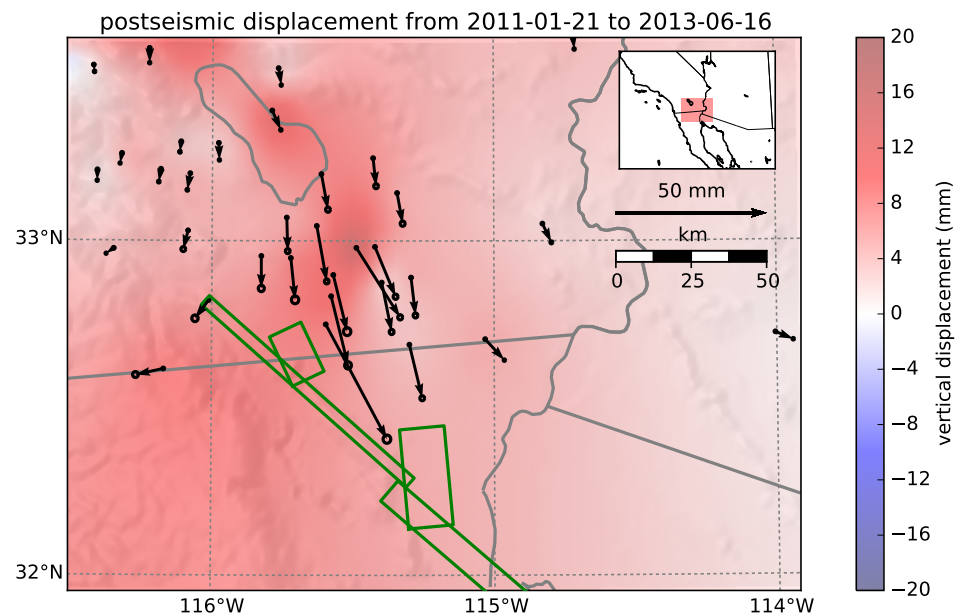


Figure 7: near field coseismic

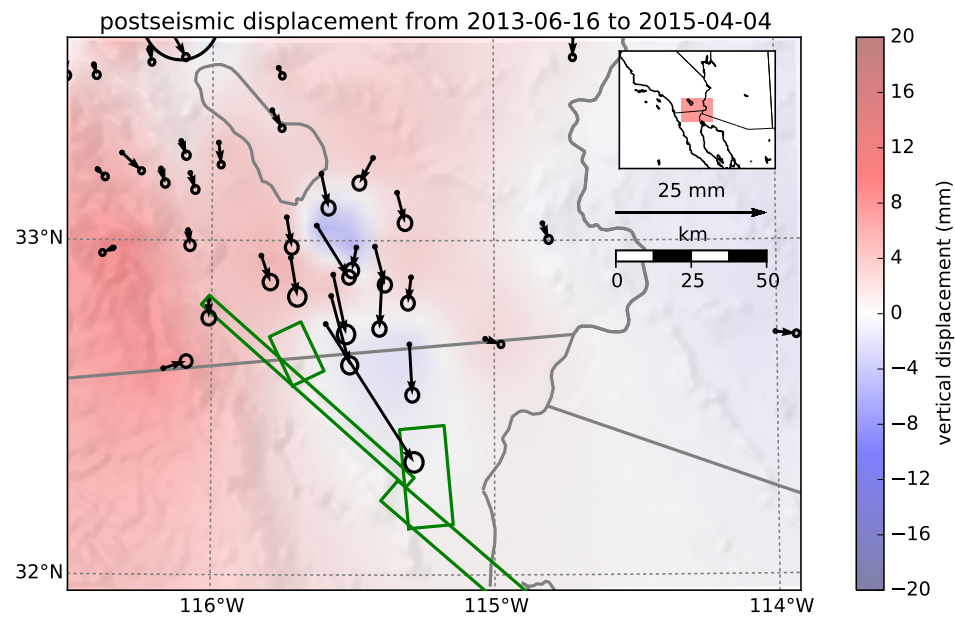


Figure 8: near field coseismic

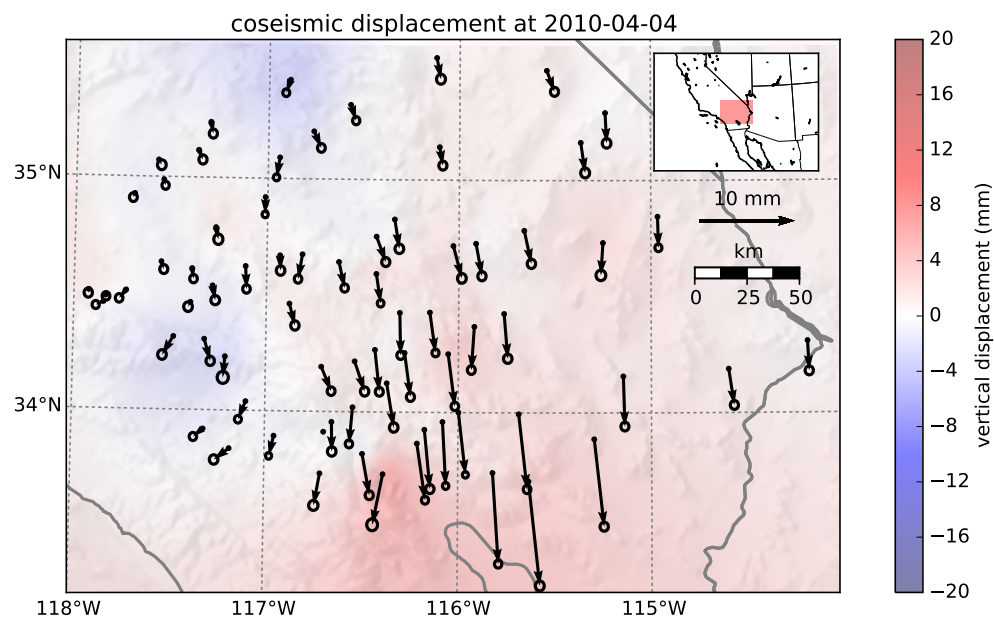


Figure 9: near field coseismic

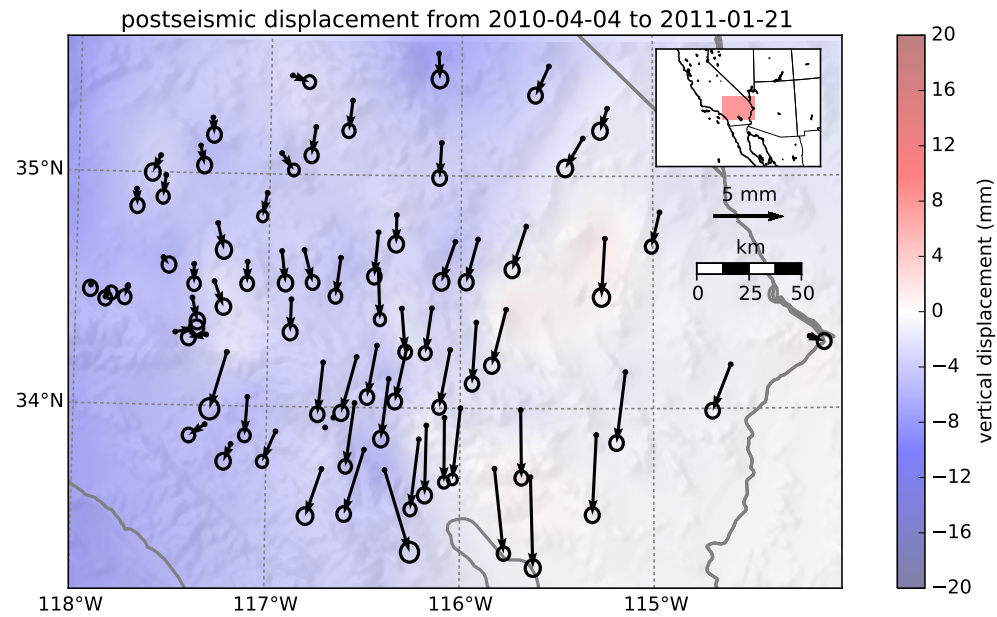


Figure 10: near field coseismic

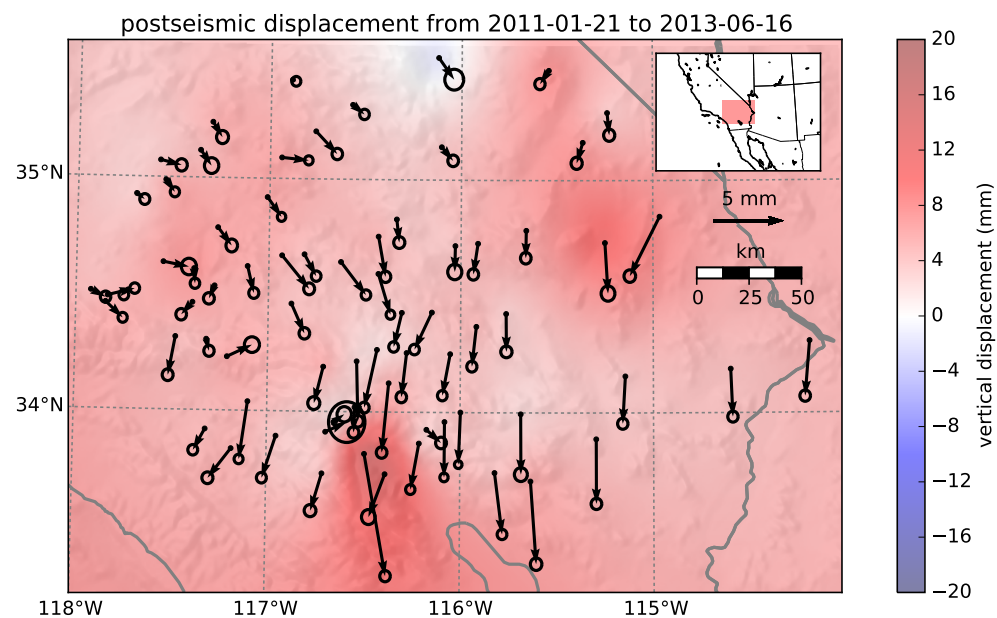


Figure 11: near field coseismic

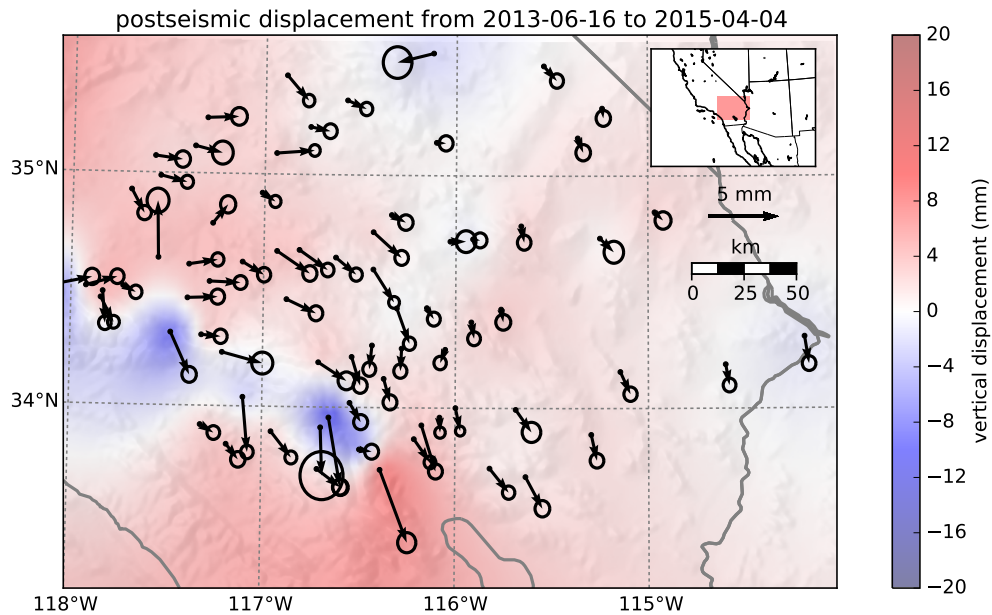


Figure 12: near field coseismic

analysis, we do not put an emphasis on trying to describe the vertical deformation as it likely has non-tectonic origins.

Near field deformation is shown in figures 6, 7, and 8. The near field deformation is notably sustained when compared to the far field deformation. Namely, the station in this study which is closest to the El Mayor-Cucapah epicenter, P496, is moving at a steady rate of 1.4 cm/yr to the south five years after the El Mayor-Cucapah earthquake. Vertical postseismic deformation in the near field does display a quadrant pattern which is consistent with the coseismic vertical deformation, suggesting that it is indeed resulting from tectonic processes. However, the vertical postseismic deformation signal is only apparent in the early postseismic period (figure 6). As with the far field deformation, there is a general trend of uplift in the near field one year after the earthquake which we do not consider to be related to postseismic processes.

Postseismic Modeling

outline:

- dismiss poroelastic rebound
- Discuss justification of afterslip as a mechanism -vertical deformation argument -Kayla's paper and Haukson
- discuss fault geometry
- Discuss viscoelastic relaxation - discuss rheologic models and parameters needed to estimate
- Discuss approximation, implications for all rheologic models -discretization of the lithosphere -discuss the nitty gritty inverse method

- issue with nonuniqueness of deep afterslip and crustal flow
- discuss fault geometry and modeling assumptions. including elastic properties. and Kayla's paper

-Discuss discretization of slip and viscosity

-discuss early postseismic approximation

In this paper, we seek to find the mechanisms driving five years of postseismic deformation following the El Mayor-Cucapah. We consider afterslip and viscoelastic relaxation in the lithosphere and/or asthenosphere as candidate mechanism. Poroelastic has also been used to model postseismic deformation (cite); however, the analysis of [Gonzalez-ortega et al., 2014] suggests found that any contribution to postseismic deformation from poroelastic rebound would be negligible. Additionally, we are considering stations which are sufficiently far away from the main rupture that poroelastic rebound should be insignificant.

In this study we estimate coseismic and time dependent postseismic fault slip, both which are assumed to occur on the fault geometry estimated by [Wei et al., 2011a] with some modifications. Field studies and other coseismic slip models have found a significantly more complicated geometry for the coseismically ruptured fault [Fletcher and Spelz, 2009] [Oskin et al., 2012]; however, the relatively simple coseismic fault geometry from [Wei et al., 2011a] is sufficient to describe the data in this study because most of the stations used here are sufficiently far from the epicenter that they are insensitive to the detailed fault geometry found by [Fletcher and Spelz, 2009] and [Oskin et al., 2012]. We do, however, modify the fault geometry from [Wei et al., 2011a] by extending segment 2 northward by 40 km which is motivated by the clustering of aftershocks on the northern tip of coseismic rupture zone [Kroll et al., 2013] [Hauksson et al., 2011]. This extended fault segment was also found to be necessary by [Rollins et al., 2015] and [Pollitz et al., 2012] for describing postseismic deformation. in the intended to account to slip

To model postseismic deformation we must first assume a rheologic model. The simplest viscoelastic rheologic model would be a Maxwell model, where shear stresses and strains can be described with the mechanical analogy of a spring and dashpot connected in series. If coseismic and postseismic slip, described by $s(\xi, t)$, occurs on a fault F , and viscoelastic relaxation of subsequent stresses occurs in a Maxwell viscoelastic medium L , which has a spatially variable viscosity, $\eta(\zeta)$, then coseismic and postseismic deformation can be described by

$$u(x, t) = \int_F s(\xi, t)g(x, \xi)d\xi + \int_0^t \int_F s(\tau, \xi)f(t - \tau, x, \xi)d\xi d\tau \quad (9)$$

where $g(x, \xi)$ is the elastic Green's function relating slip at ξ to instantaneous displacement at x and $f(t, x, \xi)$ describes the rate of deformation at x and time t resulting from viscoelastic relaxation of stresses induced by slip at ξ . The variables which we are primarily concerned with estimating in this study are $s(\xi, t)$ and $\eta(\zeta)$. Numerous experimental and geophysical studies suggest that a Maxwell rheology is inappropriate to describe the behaviour of the uppermost mantle [Chopra, 1997] [Pollitz, 2003] [Freed and Bürgmann, 2004] and so we do not limit ourselves to exploring Maxwell viscoelasticity. When considering other stress-linear viscoelastic models, such as a Zener or Burgers model, the description of displacements remains unchanged from eq 9 except that f is parameterized by additional rheologic parameters which must also be estimated. The difficulty in determining an appropriate rheologic

model and then estimating $s(\xi, t)$ and the unknown rheologic parameters from observations of $u(x, t)$ is that it is a nonlinear inverse problem with many unknown parameters and a computationally expensive forward problem. We can greatly simplify the inverse problem by first considering the early postseismic period where we can approximate $u(x, t)$ for any stress-linear viscoelastic rheology as

$$u(x, t) = \int_F s(\xi, t) g(x, \xi) d\xi + \int_0^t \int_F \int_L \frac{s(\tau, \xi)}{\eta_{\text{eff}}(\zeta)} h(x, \xi, \zeta) d\zeta d\xi d\tau \quad (10)$$

It can be shown ([Hines and Hetland, 2015]), other rheologic models in this study viscoelasticity is We also test rheologic models other than viscoelasticity to describe

There are numerous other parameters which are not known, but will be considered known in this study.

Inherent in f is also a stress-linear viscoelastic model. In this study we will be known while try to consider

Numerous researchers have used vertical deformation as a discriminant for discerning whether afterslip or viscoelastic relaxation is the dominant postseismic mechanism ([Hetland and Zhang, 2012] [Pollitz et al., 2012] [Rollins et al., 2015]). As noted by [Rollins et al., 2015] the uplift just north of the epicenter is suggestive of afterslip at seismogenic depths, as opposed to deeper afterslip which would predict subsidence north of the fault.

The early near field postseismic vertical deformation does show a quadrant pattern and is also consistent with the coseismic vertical deformation. Given

that would not becomes there is no longer a coherent far field deformation signal. This is in contrast to near field displacements which persists for the entire 5.0 years of data used in this study. Figure () further illustrates the difference in deformation regimes between near field and far field station.

We use a fault geometry from [Wei et al., 2011b], which was determined using teleseismic, GPS, and InSAR data.

After the El Mayor-Cucapah earthquake, additional GPS stations were installed In Baja California to record postseismic deformation with better spatial coverage. Two of the stations PTAX and PHJX were installed near the epicenter in the Cucapah Mountains. We do not include these two stations in our analysis because the geometry of the faults that ruptured during the earthquake is more complicated than our assumed fault geometry [Osokin et al., 2012] [Fletcher et al., 2014] and the near field stations would be most sensitive to error in our geometry. We also leave of these near field stations in order to avoid any near field processes which we do not consider in this paper [Gonzalez-ortega et al., 2014]. Numerous stations exhibit extraneous signals which can be

Rheological constraints

Results

Acknowledgements

This material is based on EarthScope Plate Boundary Observatory data services provided by UNAVCO through the GAGE Facility with support from the National Science Foundation (NSF) and National Aeronautics and Space Administration (NASA) under NSF Cooperative Agreement No. EAR-1261833.

References

- [Çakir et al., 2012] Çakir, Z., Ergintav, S., Özener, H., Dogan, U., Akoglu, A. M., Meghraoui, M., and Reilinger, R. (2012). Onset of aseismic creep on major strike-slip faults. *Geology*, 40(12):1115–1118.
- [Cetin et al., 2014] Cetin, E., Cakir, Z., Meghraoui, M., Ergintav, S., and Akoglu, A. M. (2014). Extent and distribution of aseismic slip on the Ismetpasa segment of the North Anatolian Fault (Turkey) from Persistent Scatterer InSAR. *Geochemistry, Geophysics, Geosystems*, 15.
- [Chopra, 1997] Chopra, P. N. (1997). High-temperature transient creep in olivine rocks. *Tectonophysics*, 279:93–111.
- [Fletcher and Spelz, 2009] Fletcher, J. M. and Spelz, R. M. (2009). Patterns of Quaternary deformation and rupture propagation associated with an active low-angle normal fault, Laguna Salada, Mexico: Evidence of a rolling hinge? *Geosphere*, 5(4):385–407.
- [Fletcher et al., 2014] Fletcher, J. M., Teran, O. J., Rockwell, T. K., Osokin, M. E., Hudnut, K. W., Mueller, K. J., Spelz, R. M., Akciz, S. O., Masana, E., Faneros, G., Fielding, E. J., Leprince, S., Morelan, A. E., Stock, J., Lynch, D. K., Elliott, A. J., Gold, P., Liu-Zeng, J., González-Ortega, A., Hinojosa-Corona, A., and González-García, J. (2014). Assembly of a large earthquake from a complex fault system: Surface rupture kinematics of the 4 April 2010 El Mayor-Cucapah (Mexico) Mw 7.2 earthquake. *Geosphere*, 10(4):797–827.
- [Freed and Bürgmann, 2004] Freed, A. M. and Bürgmann, R. (2004). Evidence of power-law flow in the Mojave desert mantle. *Nature*, 430(6999):548–551.
- [Freed et al., 2007] Freed, A. M., Bürgmann, R., and Herring, T. (2007). Far-reaching transient motions after Mojave earthquakes require broad mantle flow beneath a strong crust. *Geophysical Research Letters*, 34:1–5.
- [Gonzalez-ortega et al., 2014] Gonzalez-ortega, A., Fialko, Y., Sandwell, D., Nava-pichardo, F. A., Fletcher, J., Gonzalez-garcia, J., Lipovsky, B., Floyd, M., and Funning, G. (2014).

- El Mayor-Cucapah (Mw7.2) earthquake: early near-field postseismic deformation from InSar and GPS observations. *Journal of Geophysical Research*, 119:1482–1497.
- [Hauksson et al., 2011] Hauksson, E., Stock, J., Hutton, K., Yang, W., Vidal-Villegas, J. A., and Kanamori, H. (2011). The 2010 Mw 7.2 El mayor-cucapah earthquake sequence, Baja California, Mexico and Southernmost California, USA: Active seismotectonics along the Mexican pacific margin. *Pure and Applied Geophysics*, 168(3918):1255–1277.
- [Hetland and Zhang, 2014] Hetland, E. A. and Zhang, G. (2014). Effect of shear zones on post-seismic deformation with application to the 1997 Mw 7.6 manyi earthquake. *Geophysical Journal International*, 198:259–269.
- [Hines and Hetland, 2013] Hines, T. T. and Hetland, E. A. (2013). Bias in estimates of lithosphere viscosity from interseismic deformation. *Geophysical Research Letters*, 40(16):4260–4265.
- [Hines and Hetland, 2015] Hines, T. T. and Hetland, E. A. (2015). Rapid and simultaneous estimation of fault slip and heterogeneous lithospheric viscosity from post-seismic deformation. *Geophysical Journal International*, 204(1):569–582.
- [Kroll et al., 2013] Kroll, K. A., Cochran, E. S., Richards-Dinger, K. B., and Sumy, D. F. (2013). Aftershocks of the 2010 Mw 7.2 El Mayor-Cucapah earthquake reveal complex faulting in the Yuha Desert, California. *Journal of Geophysical Research: Solid Earth*, 118(October):6146–6164.
- [Osokin et al., 2012] Osokin, M. E., Arrowsmith, J. R., Hinojosa Corona, A., Elliott, A. J., Fletcher, J. M., Fielding, E. J., Gold, P. O., Gonzalez Garcia, J. J., Hudnut, K. W., Liu-Zeng, J., and Teran, O. J. (2012). Near-field deformation from the El Mayor-Cucapah earthquake revealed by differential LIDAR. *Science*, 335(6069):702–705.
- [Pollitz, 2003] Pollitz, F. F. (2003). Transient rheology of the uppermost mantle beneath the Mojave Desert, California. *Earth and Planetary Science Letters*, 215:89–104.
- [Pollitz et al., 2012] Pollitz, F. F., Bürgmann, R., and Thatcher, W. (2012). Illumination of rheological mantle heterogeneity by the M7.2 2010 El Mayor-Cucapah earthquake. *Geochemistry, Geophysics, Geosystems*, 13(6):1–17.
- [Riva and Govers, 2009] Riva, R. E. M. and Govers, R. (2009). Relating viscosities from postseismic relaxation to a realistic viscosity structure for the lithosphere. *Geophysical Journal International*, 176:614–624.
- [Rollins et al., 2015] Rollins, C., Barbot, S., and Avouac, J.-P. (2015). Postseismic Deformation Following the 2010 M7.2 El Mayor-Cucapah Earthquake : Observations , Kinematic Inversions , and Dynamic Models. *Pure and Applied Geophysics*.
- [Savage and Svare, 2009] Savage, J. C. and Svare, J. L. (2009). Postseismic relaxation following the 1992 M 7.3 Landers and 1999 M 7.1 Hector Mine earthquakes , southern California. *Journal of Geophysical Research*, 114(B01401).

- [Savage et al., 2005] Savage, J. C., Svart, J. L., and Yu, S. B. (2005). Postseismic relaxation and transient creep. *Journal of Geophysical Research: Solid Earth*, 110:1–14.
- [Segall and Mathews, 1997] Segall, P. and Mathews, M. (1997). Time dependent inversion of geodetic data. *Journal of Geophysical Research*, 102.
- [Spinler et al., 2015] Spinler, J. C., Bennett, R. A., Walls, C., Shawn, L., and Garcia, J. J. G. (2015). Assessing long-term postseismic deformation following the M7.2 4 April 2010, El Mayor-Cucapah earthquake with implications for lithospheric rheology in the Salton Trough. *Journal of Geophysical Research: Solid Earth*, 120:3664–3679.
- [Thatcher, 1983] Thatcher, W. (1983). Nonlinear Strain Buildup and the Earthquake Cycle on the San Andreas Fault. *Journal of Geophysical Research*, 88(3):5893–5902.
- [Wei et al., 2011a] Wei, M., Sandwell, D., Fialko, Y., and Bilham, R. (2011a). Slip on faults in the Imperial Valley triggered by the 4 April 2010 Mw 7.2 El Mayor-Cucapah earthquake revealed by InSAR. *Geophysical Research Letters*, 38(January):1–6.
- [Wei et al., 2011b] Wei, S., Fielding, E., Leprince, S., Sladen, A., Avouac, J.-P., Helmberger, D., Hauksson, E., Chu, R., Simons, M., Hudnut, K., Herring, T., and Briggs, R. (2011b). Superficial simplicity of the 2010 El MayorCucapah earthquake of Baja California in Mexico. *Nature Geoscience*, 4(9):615–618.